PHYSICAL REVIEW B **92**, 241304(R) (2015)

Spin chemical potential bias induced surface current evidenced by spin pumping into the topological insulator Bi_2Te_3

Faris Basheer Abdulahad,[1] Jin-Han Lin,[1] Yung Liou,[1] Wen-Kai Chiu,[1,2] Liang-Juan Chang,[1] Ming-Yi Kao,[1] Jun-Zhi Liang,[3,*] Dung-Shing Hung,[4] and Shang-Fan Lee[1,2,†]

[1]*Institute of Physics, Academia Sinica, Taipei 11529, Taiwan*

[2]*Graduate Institute of Applied Physics, National Chengchi University, Taipei 11605, Taiwan*

[3]*Department of Physics, Fu Jen Catholic University, Taipei 24205, Taiwan*

[4]*Department of Information and Telecommunications Engineering, Ming Chuan University, Taoyuan City 33348, Taiwan*

(Received 5 October 2015; published 23 December 2015)

A spin chemical potential bias can induce a spin-polarized current by the exchange interaction of a ferromagnet with the spin-momentum locking surface states of the topological insulators. We carried out our ferromagnetic resonance experiment in a NiFe/Bi_2Te_3 heterostructure. Apart from the enhanced Gilbert damping constant, we observed strong enhancement of the effective magnetic field at low temperatures. The enhanced field decreased exponentially with increasing temperature at an energy scale of 2.5 meV, representing the strength of the exchange coupling. We attribute the enhanced field to the induced spin-polarized current in the surface states of Bi_2Te_3.

DOI: 10.1103/PhysRevB.92.241304 PACS number(s): 76.50.+g, 72.25.Dc, 73.40.−c, 75.76.+j

Spin-polarized current played a major role in the debut of spintronics, including giant magnetoresistance, tunneling magnetoresistance, and spin transfer torque effects, etc. [1]. In recent works, pure spin current in which the flow of spin angular momentum is accompanied by balanced charge flow is promising due to its potential in the applications of energy efficient electronic technologies, such as magnetic memories and computing devices [1–5]. In this regard, generation, manipulation, and detection of a spin current are essential techniques for active control and manipulation of the spin degree of freedom in solid-state systems [6].

Among currently available methods that generate pure spin currents [7–12], the spin-pumping effect is widely adopted due to the high spin current intensity it can produce [7–9]. Spin pumping is achieved by generating pure spin current from a ferromagnetic (FM) layer into paramagnetic metals (PMs) [13–17], semiconductors [18–20], graphene [21], organic materials [22], and oxides, such as ZnO [23]. When the FM layer is under the ferromagnetic resonance (FMR) condition, it generates strong spin chemical potential bias, and the spin angular momentum can be transferred from the precessing magnetization to the adjacent PM, which is a pure spin current. It is further transduced into a charge current by the inverse spin Hall effect (ISHE) resulting from the spin-orbit coupling in the PM layer, which gives rise to a voltage difference. The spin-pumping process was predicted to involve a backdiffusion of the injected spins, which can modify the magnetization dynamics of the FM in three aspects: modifying the damping constant, the gyromagnetic ratio, and the effective magnetic field [24]. Although the modification of the damping constant has been found in several FM/PM spin pumping experiments [7,25–27], the other effects were estimated to be too small to have significant effects on the magnetization dynamics [24].

A topological insulator (TI), a class of the quantum state of matter, is characterized by the peculiar boundary [surface of three-dimensional (3D)/edge of two-dimensional] states that show up due to a topological character of the bulk wave function [28–30]. The time-reversal symmetry protected boundary states exhibit a massless linear dispersion relation, a lack of electron backscattering, and spin-momentum locking, i.e., spins in these states are locked perpendicularly to the momentum vector. These materials with helical spin polarization are ideal for spin current flow and may enable possible applications in spintronics.

Spin pumping from a ferromagnet into TI materials has attracted efforts to examine the TIs for an expected enhancement of the resultant spin current. Shiomi *et al.* showed that the ferromagnetic resonance linewidth ΔH of permalloy was enhanced due to the spin pumping into a $Bi_{1.5}Sb_{0.5}Te_{1.7}Se_{1.3}$ topological insulator [31]. This result clearly demonstrates the modification of the damping constant α according to the relation $\Delta H = \Delta H_0 + 4\pi f_r \alpha/\gamma$ [8,32]. For FM/TI/FM trilayers, it has been recently demonstrated that the TI can be a high capacity spin sink, and the dynamic coupling of the FM magnetizations can be observed through thin TI layers [33].

Garate and Franz [34] showed theoretically that an extra contribution to the effective magnetic field may exist in the TI/FM heterostructure. The origin of this additional contribution is the topological counterpart of the inverse spin-galvanic effect (ISGE) [35]. When a FM thin film with perpendicular anisotropy is placed on top of a TI, a quantum Hall current arising from an external electric field may, due to the ISGE, modify the effective anisotropy field.

In this Rapid Communication, we present the study of spin pumping from $Ni_{80}Fe_{20}$ into Bi_2Te_3 and show experimental evidence of the modification of the effective magnetic field. We propose that the spin-pumping-induced surface current in TI has a similar effect as the quantum Hall current mentioned above and gives rise to effective magnetic fields due to the exchange coupling. The effective field shows a strong dependence on temperature and on the TI layer thickness.

Our FM/TI samples consist of a NiFe layer with a fixed thickness of 40 nm and a Bi_2Te_3 layer with different thicknesses. The Bi_2Te_3 layer was grown on a sapphire substrate ($8 \times 4\,mm^2$) by molecular-beam epitaxy with two-steps growth and postannealing. The NiFe layer was sputtered

*phys2021@mail.fju.edu.tw
†leesf@phys.sinica.edu.tw

 ©2015 American Physical Society

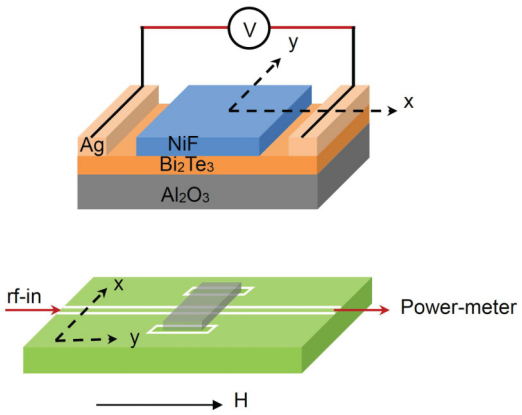

FIG. 1. (Color online) Experimental setup and sample configuration. The external magnetic field H_{dc} is pointing along the $+y$ direction.

onto the Bi_2Te_3 using a shadow mask that allows the NiFe to be grown on the center part of the Bi_2Te_3 layer, leaving $2 \times 4\,mm^2$ on each side for preparing electrodes as shown in Fig. 1. The TI-layer thickness is zero for the reference sample and 10, 15, 20, and 30 nm for the BT10, BT15, BT20, and BT30 samples, respectively.

Temperature-dependent resistivity measured by Quantum Design's physical property measurement system under a zero magnetic field shows a metallic behavior for all samples. The resistivities are about 4.3×10^{-4} and $2.3 \times 10^{-4}\,\Omega\,cm$ at room temperature and at $T = 5\,K$, respectively, which are comparable to doped semiconducting materials. From Hall voltage measurements at $T = 5\,K$, the carrier concentration was determined to be on the order of $7 \times 10^{19}\,cm^{-3}$ for our samples. This implies that the Fermi level E_F lies in the conduction band.

The experimental setup for FMR measurements consists of a coplanar waveguide circuit and a magnet. The coplanar waveguide was connected to an rf-signal generator (Rohde & Schwarz) that generates rf signals in the frequency range of 100 kHz–20 GHz. The output signal from the coplanar waveguide was connected to a power meter (Agilent E4419B-EPM series). The external dc magnetic field was produced by either an electromagnet for room-temperature measurements or by a superconducting magnet in the cryogenic probe station chamber (LakeShore, CPX-HF) for the temperature range of 4.2–300 K. The sample was mounted upside down onto the coplanar waveguide circuit using the flip-chip technique, and electrical contacts were made on the two ends of the Bi_2Te_3 layer as shown in Fig. 1. During the measurement, an external dc magnetic field was applied on the sample plane along the waveguide, and the signal generator produced microwave signals at a given frequency with a fixed power. FMR spectra were measured by connecting the coplanar waveguide to a vector network analyzer (Agilent, E8364C-PNA Microwave Network Analyzer) in order to determine the resonance frequency (f_{res}) at selective dc fields. By varying the applied dc magnetic fields, FMR spectra were measured in sequence and the magnetic-field-dependent resonance frequencies were established. Meanwhile, the dc voltage perpendicular to the magnetic field was measured on Bi_2Te_3 using a nanovoltmeter (Keithley 2182A).

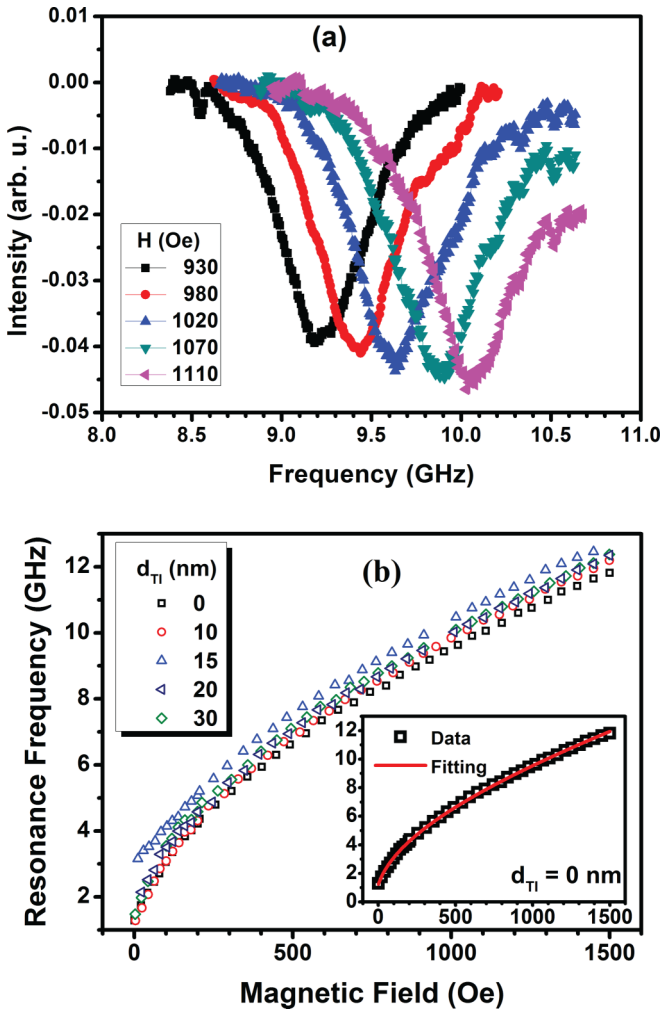

FIG. 2. (Color online) (a) FMR spectra of BT10 at $T = 5\,K$. (b) Resonance frequency as a function of external magnetic field at $T = 5\,K$. The inset shows the data fitted by the Kittel equation for the reference sample.

Figure 2(a) presents the FMR spectra of BT10 in the frequency domain measured at $T = 5\,K$. The resonance frequency increases with the external magnetic field. Clear linewidth broadening of TI/FM samples with respect to the NiFe (40-nm) reference sample (not shown) was observed due to the spin-pumping effect [36]. Figure 2(b) shows the resonance frequencies of the FMR spectra at $T = 5\,K$ as a function of the external magnetic field for all TI/FM samples along with the reference sample. The resonance frequency at a given dc magnetic field increases with TI thickness from $d_{TI} = 0$ to 15 nm, then it decreases upon further increasing of d_{TI}. Fitting these data by the Kittel equation [37],

$$f_{res} = \frac{\gamma}{2\pi}\sqrt{H_{FMR}(H_{FMR} + 4\pi M_S)}, \qquad (1)$$

where γ is the gyromagnetic ratio, M_S is the saturation magnetization, the resonance field is $H_{FMR} = H_0 + H_{eff}$, H_0 is the external magnetic field, and the effective magnetic field H_{eff} can be extracted (see the Supplemental Material for fitting details [38]). The shift of the resonance frequency can also result

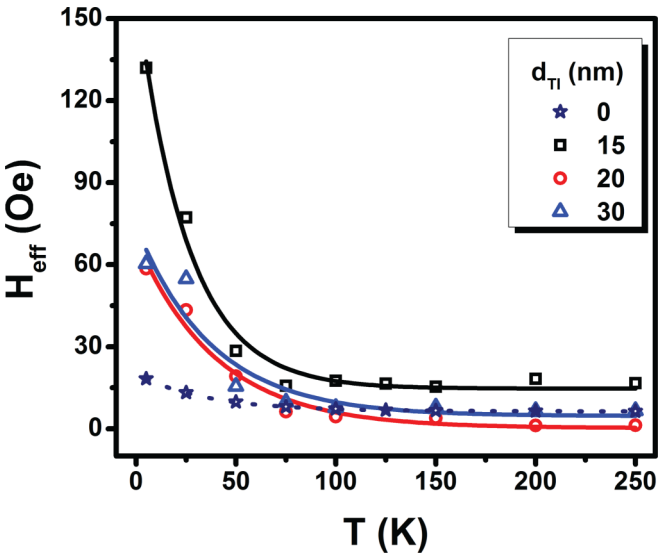

FIG. 3. (Color online) Temperature dependence of the effective magnetic fields for the reference samples BT15, BT20, and BT30. The solid lines are exponential fits.

from increasing γ or M_S. In our fittings, the former does not produce a good fit, and the latter gives unreasonably large M_S.

Temperature dependence of H_{eff} for BT15, BT20, and BT30 is displayed in Fig. 3. We note that H_{eff} declines exponentially with increasing temperature. The solid lines in the figure are fits to the data to $\exp(-T/T_0)$ form. The characteristic temperatures for T_0 are $25 \pm 2, 33 \pm 3, 30 \pm 7$ K, which correspond to the energy scale $k_B T$ of 2.2 ± 0.2, 2.8 ± 0.3, and 2.6 ± 0.6 meV, for the three samples, respectively. The dashed line in Fig. 3 shows the results for the reference sample with only an 18-Oe increase at low temperatures. In comparison, we also study the temperature dependence of the NiFe/Pt (20-nm) (FM/PM) bilayers sputtered onto Al_2O_3 substrates. It showed merely a 12-Oe increase in H_{eff} at 5 K. The increments in the reference sample and the NiFe/Pt bilayers can be attributed to the FM-layer anisotropy and the spin backflow effect. Therefore, the H_{eff} enhancement presented in FM/TI samples should arise from the employment of the TI layer.

We attribute the origin of the H_{eff} enhancement and its temperature dependence to the spin chemical potential bias and the exchange coupling between the surface state of the TI and the FM layers. Since it is difficult to fabricate high quality TI films with only surface conduction states, the spin chemical potential bias due to the spin-pumping effect can generate two separate spin currents along the surface and into the bulk of the TI. Jiao and Bauer [24] reported that when the FM layer magnetization is precessing under the resonance condition, it will generate pure dc and ac spin currents across the interface into the adjacent PM. The dc component flows along the transverse direction of the precession axis due to a spin chemical potential bias at the interface. This spin bias will decay in two opposite directions; forward into the PM layer and backward into the FM layer itself. The latter is called the spin backflow. The backflow spin current was predicted to be able to modify the FM magnetization by changing the damping constant, the gyromagnetic ratio, and the effective field. The enhancement of H_{eff} due to spin backflow was predicted to be very small. Our measurements on the NiFe/Pt and the NiFe/Al_2O_3 samples support this prediction. Recently, a well-developed quantum Hall effect arising from topological surface states in an intrinsic 3D $BiSbTeSe_2$ has been observed [39]. Transport studies of Bi_2Te_3 and Bi_2Se_3 have revealed various quantum interference phenomena confirming the existence of topological surface states in these TI materials even after exposing the samples to air and subjecting them to microelectronic treatment [40–44]. These surface states can couple to the FM layer and enhance the effective field in our experiments. We observed that this enhancement occurred only at low temperatures where the surface states of the topological insulator dominate. At high temperatures, the effective field decreased to the level comparable to that of the bare ferromagnetic sample within the experimental error. Thus, we believe the Bi_2Te_3 bulk contribution to H_{eff} is small.

The spin chemical potential bias can induce a charge current j_C in the surface states of the TI due to spin-momentum locking. The H_{eff} resulting from the induced current and the exchange coupling Δ between the surface states of the TI and the local moments of the FM layer can be written phenomenologically as

$$\mathbf{H}_{\text{eff}} \propto \Delta \hat{z} \times \mathbf{j}_C,$$

where $\hat{z}$ is the unit vector normal to the surface of the TI. The Hamiltonian of the exchange coupling for the surface states can be expressed as [34]

$$\hat{H}_{ex} = v_F \vec{\sigma}(\vec{a} \times \hat{z}) - \frac{E_{ex}}{M} \vec{\sigma} \cdot n(r), \tag{2}$$

where v_F is the surface electron Fermi velocity, $\vec{\sigma}$ is the electron spin density, and E_{ex} is the exchange-coupling energy. $\vec{a} = (E_{ex} S/e v_F M)\hat{z} \times \vec{M}$ is the effective vector potential resulting from the exchange coupling. Garate and Franz [34] pointed out theoretically that on the quantum Hall surface states of the TI where M is perpendicular to the surface, in the presence of a Hall current by $\mathbf{j}_H = \sigma_H \hat{z} \times \mathbf{E}$, with σ_{H} as the Hall conductivity and $\mathbf{E}$ as the external electric field, the additional contribution to the magnetic field is given by $\mathbf{H} = (\Delta/e v_F M_{2D})\hat{z} \times \mathbf{j}_H$. Here, e is the elementary charge, and M_{2D} is the areal magnetization at the interface. In our spin-pumping experiment, the external magnetic field defined the spin-up direction, the spin-momentum locking is required, and the induced charge current replaces the Hall current. The resulting H_{eff} has qualitatively the same form.

The dc voltage spectra we measured across the TI perpendicular to the magnetic field can be separated into symmetric and asymmetric parts. The symmetric part is of interest here and has three contributions: the induced surface state current, the ISHE current due to the spin-orbit coupling in the bulk TI, and the magnonic charge pumping (MCP) effect in the FM [45]. It is difficult to separate out these three contributions. As the FM layer is driven into FMR, pure spin current I_s is injected into the bulk TI layer where it is converted into a charge current I_c, and thus an ISHE voltage can be measured at the sample's edges. Azevedo *et al.* [46] showed that NiFe fulfills the requirement of Rashba spin-orbit coupling, and the MCP effect can give rise to a voltage in a single NiFe layer deposited onto a Si substrate.

The amplitudes of the symmetry part of the voltages are determined to be on the order of 2–5 μV. If we assume that the voltages are simply due to the bulk ISHE of the TI, the upper bound of the spin mixing conductance $g_{\uparrow\downarrow}$ can be calculated to be $1-4 \times 10^{19}\,\mathrm{m}^{-2}$. The values of the spin current density j_s time $(2e/\hbar)$ are about $1.5 \times 10^6\,\mathrm{A\,m}^{-2}$ for all samples, which are comparable to those reported for Bi_2Se_3 [47]. Finally, the spin Hall angle θ_{SH} can be determined with $\lambda_{\mathrm{sf}} = 9.5 \pm 0.35\,\mathrm{nm}$ [48] to get $\theta_{\mathrm{SH}} = 0.0062 \pm 0.001$ and 0.003 ± 0.0001 for samples with $d_{\mathrm{TI}} = 15$ and 30 nm, respectively, which are close to those reported values [48,49]. However, all these quantities should be smaller due to the MCP contribution, etc., to the voltage in our samples.

To conclude, we have studied the FMR and spin-pumping effect in the ferromagnet NiFe/topological insulator Bi_2Te_3 heterostructures at different temperatures. The effective magnetic field is enhanced and declines exponentially with temperature. Our results show that this effect is mainly due to the induced surface current resulting from the exchange interaction of the ferromagnet with the topological insulator surface states. The exchange energy is on the order of a few meV in our samples.

This work was financially supported by the Ministry of Science and Technology and the Academia Sinica of Taiwan, Republic of China.

[1] I. Zutic, J. Fabian, and S. D. Sarma, Rev. Mod. Phys. **76**, 323 (2004).
[2] S. A. Wolf, D. D. Awschalom, R. A. Buhrman, J. M. Daughton, S. von Molnar, M. L. Roukes, A. Y. Chtchelkanova, and D. M. Treger, Science **294**, 1488 (2001).
[3] *Concepts in Spin Electronics*, edited by S. Maekawa (Oxford University Press, Oxford, 2006).
[4] C. Chappert, A. Fert, and F. N. V. Dau, Nature Mater. **6**, 813 (2007).
[5] D. D. Awschalom and M. E. Flatte, Nat. Phys. **3**, 153 (2007).
[6] F. J. Jedema, A. T. Filip, and B. J. van Wees, Nature (London) **410**, 345 (2001).
[7] K. Ando and E. Saitoh, Nat. Commun. **3**, 629 (2012).
[8] K. Ando, S. Takahashi, K. Harii, K. Sasage, J. Ieda, S. Maekawa, and E. Saitoh, Phys. Rev. Lett. **101**, 036601 (2008).
[9] Y. Kajiwara, K. Harii, S. Takahashi, J. Ohe, K. Uchida, M. Mizuguchi, H. Umezawa, H. Kawai, K. Ando, K. Takanashi, S. Maekawa, and E. Saitoh, Nature (London) **464**, 262 (2010).
[10] T. Kikkawa, K. Uchida, Y. Shiomi, Z. Qiu, D. Hou, D. Tian, H. Nakayama, X. F. Jin, and E. Saitoh, Phys. Rev. Lett. **110**, 067207 (2013).
[11] D. Qu, S. Y. Huang, J. Hu, R. Wu, and C. L. Chien, Phys. Rev. Lett. **110**, 067206 (2013).
[12] B. F. Miao, S. Y. Huang, D. Qu, and C. L. Chien, Phys. Rev. Lett. **111**, 066602 (2013).
[13] Y. Tserkovnyak, A. Brataas, and G. E. W. Bauer, Phys. Rev. Lett. **88**, 117601 (2002).
[14] R. Urban, G. Woltersdorf, and B. Heinrich, Phys. Rev. Lett. **87**, 217204 (2001).
[15] S. Mizukami, Y. Ando, and T. Miyazaki, J. Magn. Magn. Mater. **226-230**, 1640 (2001).
[16] O. Mosendz, J. E. Pearson, F. Y. Fradin, G. E. W. Bauer, S. D. Bader, and A. Hoffmann, Phys. Rev. Lett. **104**, 046601 (2010).
[17] A. Azevedo, L. H. Vilela-Leão, R. L. Rodríguez-Suárez, A. F. Lacerda Santos, and S. M. Rezende, Phys. Rev. B **83**, 144402 (2011).
[18] K. Ando, S. Takahashi, J. Ieda, H. Kurebayashi, T. Trypiniotis, C. H. W. Barnes, S. Maekawa, and E. Saitoh, Nature Mater. **10**, 655 (2011).
[19] L. Chen, F. Matsukura, and H. Ohno, Nat. Commun. **4**, 2055 (2013).
[20] H. Y. Hung, T. H. Chiang, B. Z. Syu, Y. T. Fanchiang, J. G. Lin, S. F. Lee, M. Hong, and J. Kwo, Appl. Phys. Lett. **105**, 152413 (2014).
[21] Z. Tang, E. Shikoh, H. Ago, K. Kawahara, Y. Ando, T. Shinjo, and M. Shiraishi, Phys. Rev. B **87**, 140401 (2013).
[22] K. Ando, S. Watanabe, S. Mooser, E. Saitoh, and H. Sirringhaus, Nature Mater. **12**, 622 (2013).
[23] J. C. Lee, L. W. Huang, D. S. Hung, T. H. Chiang, J. C. A. Huang, J. Z. Liang, and S. F. Lee, Appl. Phys. Lett. **104**, 052401 (2014).
[24] H. J. Jiao and G. E. W. Bauer, Phys. Rev. Lett. **110**, 217602 (2013).
[25] T. Yokoyama, J. Zang, and N. Nagaosa, Phys. Rev. B **81**, 241410(R) (2010).
[26] K. Ando, S. Takahashi, J. Ieda, Y. Kajiwara, H. Nakayama, T. Yoshino, K. Harii, Y. Fujikawa, M. Matsuo, S. Maekawa, and E. Saitoh, J. Appl. Phys. **109**, 103913 (2011).
[27] A. K. Patra, S. Singh, B. Barin, Y. Lee, J. H. Ahn, E. del Barco, E. R. Mucciolo, and B. Özyilmaz, Appl. Phys. Lett. **101**, 162407 (2012).
[28] M. Z. Hasan and C. L. Kane, Rev. Mod. Phys. **82**, 3045 (2010).
[29] X.-L. Qi and S.-C. Zhang, Rev. Mod. Phys. **83**, 1057 (2011).
[30] Y. Ando, J. Phys. Soc. Jpn. **82**, 102001 (2013).
[31] Y. Shiomi, K. Nomura, Y. Kajiwara, K. Eto, M. Novak, K. Segawa, Y. Ando, and E. Saitoh, Phys. Rev. Lett. **113**, 196601 (2014).
[32] F. B. Abdulahad, D. S. Hung, Y. C. Chiu, and S. F. Lee, IEEE Trans. Magn. **47**, 4227 (2011).
[33] A. A. Baker, A. I. Figueroa, L. J. Collins-McIntyre, G. van der Laan, and T. Hesjedal, Sci. Rep. **5**, 7907 (2015).
[34] I. Garate and M. Franz, Phys. Rev. Lett. **104**, 146802 (2010).
[35] E. L. Ivchenko and S. Ganichev, *Spin Physics in Semiconductors*, edited by M. I. Dyakonov (Springer, New York, 2008).
[36] A. Azevedo, L. H. V. Leao, R. L. Rodriguez-Suarez, A. B. Oliveira, and S. M. Rezende, J. Appl. Phys. **97**, 10C715 (2005).
[37] F. B. Abdulahad, D. S. Hung, and S. F. Lee, J. Metab. Res. **29**, 1237 (2014).
[38] See Supplemental Material at http://link.aps.org/supplemental/10.1103/PhysRevB.92.241304 for fitting details.

[39] Y. Xu, I. Miotkowski, C. Liu, J. Tian, H. Nam, N. Alidoust, J. Hu, C. K. Shih, M. Z. Hasan, and Y. P. Chen, Nat. Phys. **10**, 956 (2014).

[40] D. X. Qu, Y. S. Hor, J. Xiong, R. J. Cava, and N. P. Ong, Science **329**, 821 (2010).

[41] H. Peng, K. Lai, D. Kong, S. Meister, Y. Chen, X.-L. Qi, S.-C. Zhang, Z.-X. Shen, and Y. Cui, Nature Mater. **9**, 225 (2010).

[42] J. G. Checkelsky, Y. S. Hor, R. J. Cava, and N. P. Ong, Phys. Rev. Lett. **106**, 196801 (2011).

[43] J. Chen, H. J. Qin, F. Yang, J. Liu, T. Guan, F. M. Qu, G. H. Zhang, J. R. Shi, X. C. Xie, C. L. Yang, K. H. Wu, Y. Q. Li, and L. Lu, Phys. Rev. Lett. **105**, 176602 (2010).

[44] J. G. Checkelsky, Y. S. Hor, M.-H. Liu, D.-X. Qu, R. J. Cava, and N. P. Ong, Phys. Rev. Lett. **103**, 246601 (2009).

[45] C. Ciccarelli, K. M. D. Hals, A. Irvine, V. Novak, Y. Tserkovnyak, H. Kurebayashi, A. Brataas, and A. Ferguson, Nat. Nanotechnol. **10**, 50 (2014).

[46] A. Azevedo, R. O. Cunha, F. Estrada, O. Alves Santos, J. B. S. Mendes, L. H. Vilela-Leão, R. L. Rodríguez-Suárez, and S. M. Rezende. Phys. Rev. B **92**, 024402 (2015).

[47] M. Jamali, J. S. Lee, Y. Lv, Z. Zhao, N. Samarth, and J. P. Wang, arXiv:1407.7940.

[48] P. Deorani, J. Son, K. Banerjee, N. Koirala, M. Brahlek, S. Oh, and H. Yang, Phys. Rev. B **90**, 094403 (2014).

[49] C. N. Wu, Y. H. Lin, Y. T. Fanchiang, H. Y. Hung, H. Y. Lin, P. H. Lin, J. G. Lin, S. F. Lee, M. Hong, and J. Kwo, J. Appl. Phys. **117**, 17D148 (2015).